Optical properties of the F^+ center in crystalline Al_2O_3

B. D. Evans and M. Stapelbroek
Optical Sciences Division, Naval Research Laboratory, Washington, D. C. 20375
(Received 12 June 1978)

Ultraviolet optical absorption, emission, and excitation spectra are presented for 14-MeV neutron-irradiated high-purity crystalline Al_2O_3. Low-temperature polarized excitation spectra for the 3.8-eV luminescence correlated well with polarized absorption at 4.8 eV (both polarizations) and 5.4 eV ($\vec{E} \perp \vec{c}$). These optical properties compare favorably with those predicted using wave functions from an earlier point-ion calculation for the F^+ center by La, Bartram, and Cox. The 4.8- and 5.4-eV absorption bands are assigned to the $1A \rightarrow 1B$ and $1A \rightarrow 2A$ transitions, respectively, of the F^+ center and the 3.8-eV luminescence is assigned to the $1B \rightarrow 1A$ transition. The $1A \rightarrow 2B$ transition could not be conclusively identified, but preliminary evidence suggests it occurs near 6.3 eV. Similar absorption and emission bands are observed following energetic-proton and Al^+ bombardment. Other uv optical properties are presented, including the quantum efficiency, lifetime, and temperature dependence of the emission.

I. INTRODUCTION

Changes induced by radiation in electronic, optical, and mechanical properties of crystalline alumina have been studied for some time.[1-4] Early energetic neutron and electron irradiation studies indicated the prominent optical absorption band near 6 eV is due to charges trapped at defects which occur when atoms are displayed.[3,5,6] A 13-line electron-spin-resonance spectrum found in neutron-irradiated samples has been assigned to an F^+ center, i.e., one electron trapped at an anion vacancy; however, no positive correlation was made with optical data.[7] More recently, bombardment with energetic ions has been shown to produce uv absorption bands similar to those induced by neutron irradiation in addition to near-surface expansion.[8,9] Ion implantation with oxygen and aluminum demonstrated that the uv coloration and a 3.8-eV luminescence are associated with an anion-deficient stochiometric imbalance.[10] Optical and thermal bleaching of neutron-irradiated sapphire has associated the 6-eV band with an electron-trapping site.[11] Subsequent photobleaching investigations have assigned the 6-eV band to an F center (two electrons trapped at an anion vacancy) and the 4.8-eV absorption band to the $1A \rightarrow 2A$ transition of an F^+ center possessing C_2 symmetry.[12] The present work on fusion-neutron-irradiated sapphire will demonstrate that the 4.8- and 5.4-eV absorption bands are $1A \rightarrow 1B$ and $1A \rightarrow 2A$ transitions, respectively, of the F^+ center. Most of the prominent 6-eV band is, as previously assigned by Lee and Crawford,[12] associated with an F center; however, preliminary evidence suggests that the $1A \rightarrow 2B$ transition of the F^+ center occurs as a shoulder on the 6-eV band near 6.3 eV. Such an accidental near degeneracy between F^+- and F-center transition energies is not unique; a prime example occurs in MgO where both F^+ and F centers have optical absorption near 5 eV.[13,14] Furthermore, the 3.8-eV luminescence band is associated here with a $1B \rightarrow 1A$ electric-dipole-allowed transition of the F^+ center. These assignments are in agreement with predictions made from the eigenfunctions obtained by the point-ion calculation of La, Bartram, and Cox.[7]

II. PROCEDURE

High-purity crystalline sapphire samples grown by the Czochralski technique were obtained from Union Carbide Corporation. Table I summarizes the results of a semiquantitative spectrochemical analysis. These samples were members of two groups of fusion-neutron-irradiated sapphire crystals whose initial optical absorption properties and annealing behavior were recently found similar to that reported earlier for fission-neutron-irradiated sapphire.[3,6,8] These samples were exposed to moderate doses of $(1.7\text{–}14)\times10^{16}$ 14-MeV neutrons/cm^2 at a flux of about 10^{12} neutrons/cm^2 sec at ~300 K in the Lawrence Livermore Laboratory Rotating Target Neutron Source. The absolute neutron fluence accuracy determined by niobium foil activation dosimetry is believed to be about $\pm 7.5\%$.[15]

Sapphire grown by the Czochralski technique is expected to be more suitable than Verneuil-grown material for the study of intrinsic damage effects at low and moderate damage levels because of much smaller concentrations of quenched-in defects in the as-grown material. However, substrate-grade Verneuil alumina samples obtained from Adolf Meller and Co. were considered acceptable for ion implantation damage studies where

 © 1978 The American Physical Society

TABLE I. Impurity analysis of Czochralski sapphire in ppm. The estimated precision is <50%, relative standard deviation.

Li,	<10	Mn,	<1	Mo,	<3
Be,	<1	Fe,	3	Ag,	<1
B,	<5	Co,	<5	Cd,	<3
Na,	<10	Ni,	<5	In,	<10
Mg,	3	Cu,	1	Sn,	<10
Si,	<5	Zn,	<30	Sb,	<30
K,	<100	Ga,	3	Ba,	<3
Ca,	<5	Ge,	<30	Ta,	<300
Ti,	<3	Sr,	<1	W,	<100
V,	<3	Zr,	10	Pb,	<10
Cr,	<3	Nb,	<100	Bi,	<10

the local damage concentration is much higher. The ultraviolet and vacuum ultraviolet (vuv) subgap absorption of as-received Verneuil material appears larger than that of the Czochralski crystals indicating the presence of more cation impurities.[10,16] The Verneuil samples were ion implanted near room temperature with 0.4-μA/cm^2 proton, 2-μA/cm^2 Al^+, or 0.8-μA/cm^2 O^+ ion beams at 200 keV.

Polarized optical measurements employed type 105 uv polarizing filters supplied by Polacoat, Inc. Additional measurements were facilitated by preparing crystals with the c axis either parallel or perpendicular to the direction of the incident light. Absorption measurements were taken with Cary 14MR and 17D recording spectrophotometers and a McPherson model 225 1-m vuv scanning monochromator. Luminescence and excitation spectra were measured with Bausch and Lomb 0.25-m high-intensity monochromators. The detection system used an S-20 photomultiplier tube calibrated with the use of an Electro-Optics Associates model L-101 spectral irradiance standard quartz-iodide lamp. Excitation measurements used calibrated xenon and deuterium sources. Substitution with freshly prepared sodium salicylate films was the method used to determine the luminescence quantum efficiency. Low-temperature spectra were obtained with a small stainless-steel cryostat fitted with a copper cold finger. High-temperature measurements were taken with samples mounted near a copper-Constantan thermocouple on a brass block in a small oven fitted with Suprasil 1 windows.

Radiative lifetime measurements were made using a pulsed deuterium discharge tube with a rise time (10%–90%) $\tau_r \sim 7$ nsec, a fall time $\tau_f \sim 15$ nsec, and a pulse full width at half maximum (FWHM) ~13 nsec. Response to pulsed excitation was recorded with a Hewlett-Packard type 183C oscilloscope. Emission and excitation spectra under pulsed excitation were recorded with the use of a Princeton Applied Research model 160 boxcar integrator.

III. RESULTS

A. Ultraviolet absorption and emission

Typical polarized uv absorption, emission, and excitation spectra are shown in Fig. 1 for high-purity Czochralski sapphire irradiated with 14-MeV neutrons. The background absorption spectra, taken before irradiation, suggest bands near 7.0 and 6.4 eV indicating trace impurity levels of Cr^{3+} (2 ± 1 ppm) and Fe^{3+} (0.2 ± 0.1 ppm), respectively.[16] (The *very* weak Fe^{3+} 4.8-eV band has a reported FWHM of 0.65–0.70 eV,[16] and should not be confused with the narrower particle-irradiation-induced band near the same energy.) After fusion-neutron irradiation, uv absorption bands appear near 4.8, 5.4, and 6 eV.[8] These bands become narrower and more intense at low temperature. The 5.4-eV band appears only with light polarized $\vec{E} \perp \vec{c}$; this anisotropy agrees with that found by Mitchell *et al.*[3] in fission-neutron-irradiated sapphire. In addition, the high-energy side of the 6-eV band appears stronger for $\vec{E} \parallel \vec{c}$; however, it should be noted that the 6.4-eV Fe^{3+} band may interfere.

Excitation in the 4.8- and 5.4-eV absorption bands produces a characteristic 3.8-eV luminescence band.[10] At lower temperature the emission band narrows and shifts to higher energy. In order to elucidate the origin of this luminescence, low-temperature polarized excitation spectra were taken; these are shown below the corresponding polarized absorption bands in Fig. 1. The correlation between the excitation and absorption spectra is striking; the 3.8-eV emission is most intense when pumped near 4.8 and 5.4 eV with a weaker but significant response near 6 eV. Furthermore, the response to polarized excitation very closely follows the polarized absorption for the 4.8- and 5.4-eV bands indicating the absorption and emission phenomena are related. The luminescence is not strongly polarized; its intensity depends on the polarization of the pump light as is shown by the excitation spectra. Table II summarizes the experimental information for these bands. Similar absorption and emission has been reported for ion-bombarded and fission-neutron-irradiated alumina.[10,12]

B. Emission-band temperature dependence

Figure 2 shows the temperature dependence of the emission band in greater detail. As the temperature is increased, three features are ob-

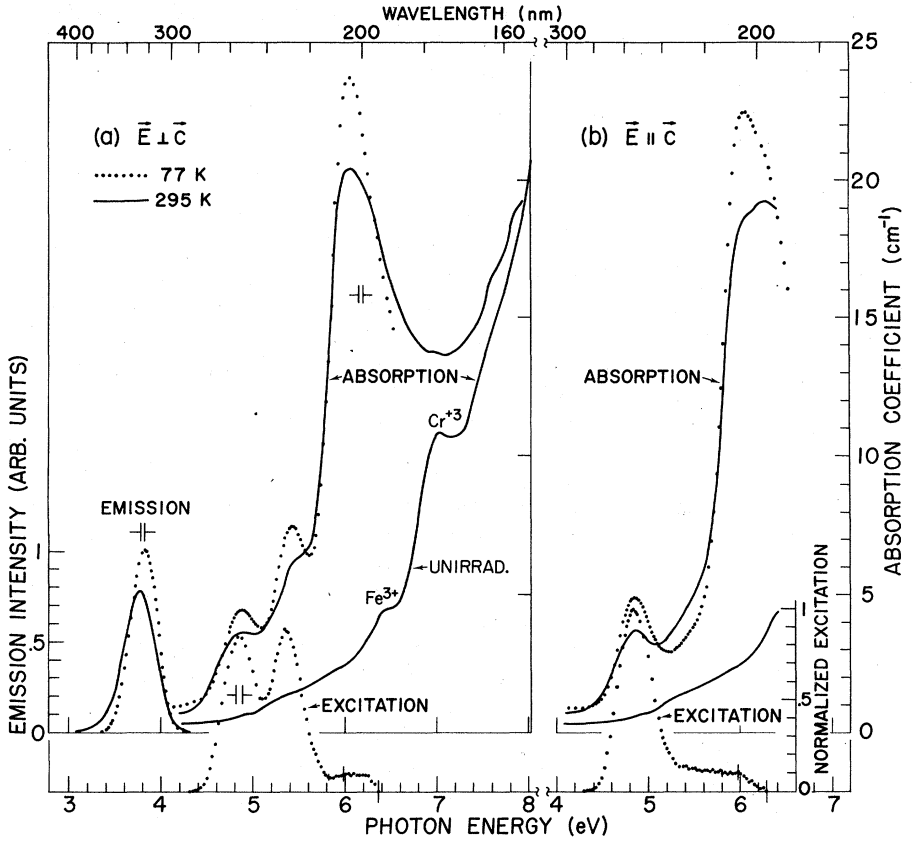

FIG. 1. Polarized optical absorption from high-purity Czochralski sapphire irradiated to 3.9×10^{16} 14-MeV neutrons/cm^2 followed by a 20-min exposure to 300°C. Emission and excitation from other samples bombarded to 1.7×10^{16} neutrons/cm^2. (a) $\vec{E} \perp \vec{c}$; (b) $\vec{E} \parallel \vec{c}$.

served: (i) the integrated intensity decreases: (ii) the band peak shifts to lower energy; (iii) the band width increases. The band shape is characterized by distribution moments; details of the moments analysis are presented in Appendix B. The temperature dependence of factors proportional to these moments is presented below.

The quantum efficiency of the luminescence is proportional to the zeroth moment; i.e., the area under the bands shown in Fig. 2. The quantum efficiency was measured by comparison with freshly prepared sodium salicylate which has a reported

TABLE II. 14-MeV neutron-induced F^+ absorption- and emission-band parameters at 77 K.

Peak position (eV) determined from Absorption	Excitation	FWHM (eV) determined from Absorption	Excitation	Transition assignment
4.85 ± 0.01	4.84 ± 0.01	$0.41\pm0.02(\vec{E}\parallel\vec{c})$	$0.44\pm0.01(\vec{E}\parallel\vec{c})$	$1A\rightarrow1B$
$5.41^{+0.01}_{-0.03}$ [a]	5.34 ± 0.02	0.32 ± 0.05 [b]	$0.43^{+0.03}_{-0.06}$ [b]	$1A\rightarrow2A$
(6.3 ± 0.2) [c]	···	(<0.8)	···	$(1A\rightarrow2B)$ [c]
6.05 ± 0.02	···	0.67 ± 0.05 [d] $(\vec{E}\perp\vec{c})$ 0.78 ± 0.1 [d] $(\vec{E}\parallel\vec{c})$	···	F center [e]
Emission		Emission		
3.82 ± 0.01	···	0.34 ± 0.01	···	$1B\rightarrow1A$

[a] May be shifted to higher energy by the long-wavelength tail of the 6-eV band.
[b] Decomposing the $\vec{E}\perp\vec{c}$ spectrum introduces a larger error.
[c] Tentative identification.
[d] FWHM for composite F and F^+ bands.
[e] Reference 12.

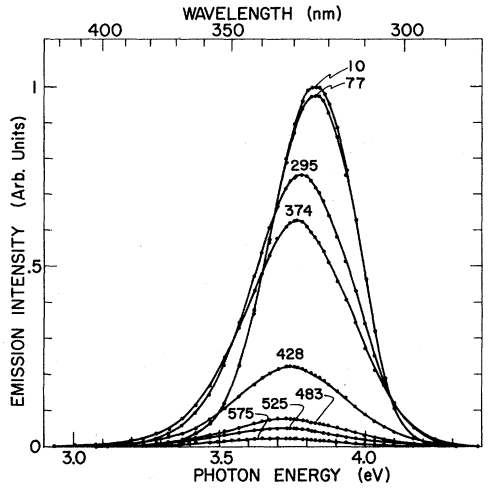

FIG. 2. Temperature (K) dependence of the 3.8-eV emission band. The excitation was centered at 257 nm with a bandwidth of 22 nm. The sample was exposed to 3.9×10^{16} neutrons/cm^2.

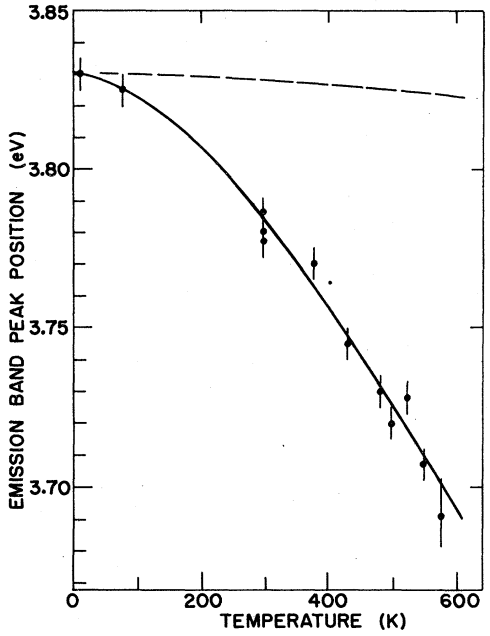

FIG. 4. Temperature dependence of the 3.8-eV emission-band peak position from Fig. 2. The dashed curve estimates the small contribution from lattice thermal expansion (see Appendix A).

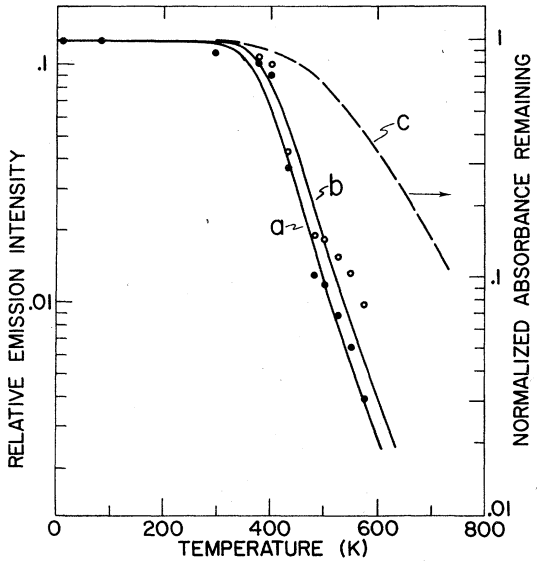

FIG. 3. Temperature-dependent integrated emission intensity relative to sodium salicylate at room temperature, from Fig. 2. The following utilize the left-hand scale: solid circles and curve (a) for the best fit of Eq. (2), with $\tau_R\nu_0=4\times10^4$ and $\Delta E=0.397$ eV; open circles and curve (b), emission corrected for centers lost due to annealing during high-temperature emission, together with the best fit to Eq. (2) with $\Delta E=0.418$ eV. Curve (c) and the right-hand scale represent isochronal anneal of the 4.8-eV absorption band taken from Ref. 8 and used to correct the emission data. Low-temperature quantum efficiency data was taken before high-temperature emission data.

quantum efficiency of 0.99 when excited with 253.7-nm radiation.[17] However, as there may be some uncertainty in the absolute fluorescent quantum efficiency of the films employed, we have chosen to present the luminescence intensity *relative* to sodium salicylate at room temperature. The temperature dependence of the integrated emission intensity is shown in Fig. 3 by the solid circles. The two salient features are a low-temperature relative quantum efficiency near 0.12 and a high-temperature "knee" near 350 K.

The emission-band peak position is related to the first moment. Figures 2 and 4 show the peak position shifting to lower energy with increasing temperature. A small contribution to this shift, shown by the dashed curve in Fig. 4, is due to the thermal expansion of the lattice. The size of this effect is estimated in Appendix A using a particle-in-a-box defect model and the related Mollwo-Ivey relation together with reported sapphire thermal expansion coefficients. As seen in Fig. 4, the lattice thermal expansion contribution is small compared to the observed shift. In addition, the temperature-dependent expression for the band centroid obtained by including higher-order coupling terms by assuming slightly different effective vibronic frequencies for ground ($1A$) and excited ($1B$) states [see Ref. 18, Chap. 7, Eq. (19)] could not account for the large observed shift.

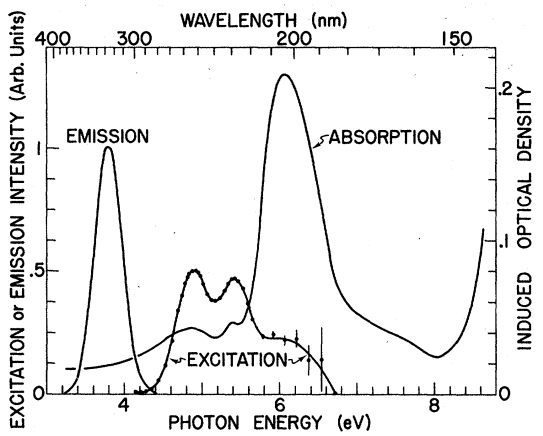

FIG. 5. Unpolarized room-temperature absorption and emission from Verneuil sapphire bombarded to 1.0×10^{16} 200-keV protons/cm^2.

C. Radiative lifetime

An attempt was made to measure the radiative lifetime of the 3.8-eV emission. Limited temporal resolution placed a least upper bound on the lifetime of $\tau_R \lesssim 7\times10^{-9}$ sec at the temperatures investigated (8, 77, and 295 K). The same results were obtained at these temperatures by pumping any of the excitation regions near 4.8, 5.4, and 6 eV. Furthermore, the shapes of the emission and excitation spectra taken under pulsed conditions were the same as measured with cw excitations, e.g., as shown in Fig. 1.

D. Effects of irradiation with other particles

Bombardment of sapphire with other energetic particles revealed additional information on the nature of the uv absorption and emission bands. Implantation of Al_2O_3 with 200-keV H^+ and Al^+ ions produced the characteristic uv-absorption bands at 4.8, 5.4, and 6 eV whereas implantation of 200-keV O^+ ions did not result in the formation of these bands.[10,19] Good correlation was again observed between absorption and the excitation spectra for the 3.8-eV emission for the H^+ and Al^+ implanted samples; Fig. 5 shows the results for the proton-bombarded case. The 3.8-eV luminescence was not observed in the O^+-implanted material. These results have been interpreted to mean that the absorption bands at 4.8, 5.4, and 6 eV are associated with a stochiometric upset in favor of excess aluminum or, conversely, oxygen vacancies.[10] In addition, the results for the emission lifetime in H^+-bombarded samples were identical to those found in the neutron-irradiated samples.

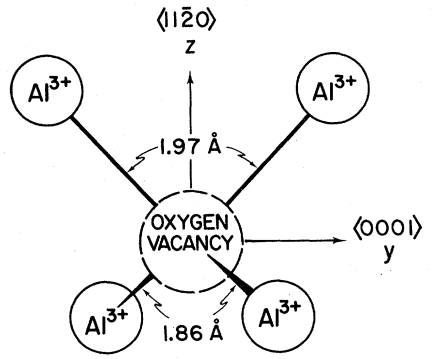

FIG. 6. Coordinate system used to describe the F^+ center in α-Al_2O_3. The x axis is out of the plane of the figure.

IV. DISCUSSION

A. Theoretical predictions

La, Bartram, and Cox[7] have calculated wave functions for the F^+ center in Al_2O_3 by the variational method using a point-ion model for the anisotropic crystal field potential and including contributions from s,p, and d functions. Because of the low symmetry (point group C_2) of the F^+ center, the three degenerate p-like excited states are split by the crystal field into states labeled $1B$, $2A$, and $2B$ which were calculated to be 2.26, 3.39, and 5.15 eV, respectively, above the $1A$ ground state.

For light polarized along the $x_j = x,y$, or z axis of the defect, the oscillator strength of the transition from $\psi_0 \rightarrow \psi_i$ is given by the formula,[20] $f_{ij} = (E_i - E_0)\,|\langle\psi_i|x_j|\psi_0\rangle|^2$, where all quantities are in Slater atomic units. Single-site oscillator strengths were calculated using the coordinate system of Fig. 6 and the wave functions given in Ref. 7. The results for light polarized along the x,y, and z axes are tabulated in Table III. The total F^+ center oscillator strength for unpolarized light is given by[20] $f = \frac{1}{3}\sum_{i,j} f_{ij} = 0.66$ which is very reasonable for a one-electron center.[20] There are six different orientations of the F^+ center in the corundum lattice; i.e., the three generated

TABLE III. Calculated oscillator strengths, $f_{ij} = (E - E_0)|\langle\psi_i|x_j|\psi_0\rangle|^2$, for light polarized along $x_j = x$, y, or z.

f_{ij}	$i=1$ $1A\rightarrow1B$	$i=2$ $1A\rightarrow2A$	$i=3$ $1A\rightarrow2B$
f_{ix}	0.601	0.0	0.013
f_{iy}	0.292	0.0	0.414
f_{iz}	0.0	0.664	0.0

TABLE IV. Comparison of observed band intensities with calculated oscillator strengths.

	$1A \rightarrow 1B$ (4.8 eV)	$1A \rightarrow 2A$ (5.4 eV)	$1A \rightarrow 2B$ (6.3 eV?)
$\vec{E} \parallel \vec{c}$	1.049 [c] (0.660) [a]	0.00 (0.0)	? b (0.935)
$\vec{E} \perp \vec{c}$	0.797 (0.905)	1.000 [c] (1.000)	? b (0.020)

[a] Calculated relative intensities derived from Table III are given in parentheses.
[b] Insufficient data.
[c] Band intensities taken as product of peak intensity and FWHM, then normalized relative to the $\vec{E} \perp \vec{c}$ 5.4-eV band.

by the site shown in Fig. 6 rotated by 0°, 120°, and 240° about the y axis, and an additional three generated by reflection of this site in the xy plane followed by 0°, 120°, and 240° rotations. Appropriate sums were taken to obtain the effective oscillator strengths for light polarized parallel and perpendicular to the c axis for each of the transitions. Properly normalized, these effective oscillator strengths give the relative band intensities expected from the point-ion wave functions. Comparison with experimental relative intensities is provided in Table IV.

B. Transition assignments

The evidence that supports assignments of the 4.8- and 5.4-eV absorption bands and the 3.8-eV emission band to the $1A \rightarrow 1B$, $1A \rightarrow 2A$, and $1B \rightarrow 1A$ transitions, respectively, of the F^+ center is summarized in this section. The evidence for the assignment of the 6-eV band to the F center is also reviewed.

The 4.8-, 5.4-, and 6-eV absorption bands have been observed following energetic neutron,[3,6] proton,[8,9] or Al^+ irradiations,[10] while the prominent 6-eV band has been observed after low-temperature, energetic ($\geq$0.75 MeV) electron irradiation.[5] However, implantation with O^+ ions or γ irradiation (see below for a discussion of the difference between the 5.4-eV band induced by γ irradiation and the particle-induced 5.4-eV band) does not result in the appearance of these bands. Because energetic particles are required to induce these bands, it has been inferred[3,5,6,10] that the defects responsible for these absorptions are primary lattice defects associated with atomic displacements. In fact, Arnold and Compton[5] have deduced the displacement threshold energy required to produce the 6-eV band by electron irradiation as 90 eV if oxygen is displaced and 50 eV if aluminum is displaced. Furthermore, the absence of these bands following O^+ ion implantation has been interpreted to mean that the defects responsible are associated with a stoichiometric imbalance in favor of excess Al or, conversely, oxygen vacancies. Taken together, these experimental facts along with previous results in other oxide materials strongly suggest that the defects responsible for the 4.8-, 5.4-, and 6-eV absorption bands and the 3.8-eV emission band are single, unassociated oxygen vacancies; i.e., F and F^+ centers ("nude" anion vacancies are not expected to be stable). Interstitial aluminum is not considered a likely cause for these absorption bands.

Lee and Crawford[12] have reported optically induced photoconversion between the 4.8- and 6-eV bands. On the basis of their results, they assign the 4.8-eV band to a transition of the F^+ center and the 6-eV band to the F center. More recently, Lee and Crawford[21] have reported observation of the 6-eV band in additively colored samples of Al_2O_3. By analogy with additive coloration results in alkaline earth oxides,[13,14,22-24] this supports the assignment of the 6-eV band to the F center.

The present study firmly identifies the transitions responsible for the 4.8- and 5.4-eV absorption and the 3.8-eV emission bands. The excitation spectra shown in Fig. 1 (along with the observation that the relative intensities of the low-temperature peaks at 4.8 and 5.4 eV do not change from sample to sample) clearly show that the 4.8- and 5.4-eV bands are different electronic transitions of the same center. Assignment of the 4.8-eV band to the $1A \rightarrow 1B$ transitions, the 5.4-eV band to the $1A \rightarrow 2A$ transition, and the 3.8-eV emission to the $1B \rightarrow 1A$ transition of the F^+ center provides excellent agreement with the theory of La, Bartram, and Cox[7] as is shown in Table IV. In conjunction with the evidence from previous investigations outlined above, the origins of the 4.8-, 5.4-, and 6-eV absorption bands and the 3.8-eV emission band are firmly established. Figure 7 is a schematic representation of these F^+-center energy level assignments.

The above assignments differ from those of Lee and Crawford.[12] They identify the 4.8-eV band with the $1A \rightarrow 2B$ F^+-center transition, the 3.8-eV luminescence with a $2B \rightarrow 1A$ transition, and the 5.4-eV absorption is assigned the same origin as the 5.4-eV band found in γ-irradiated crystals.

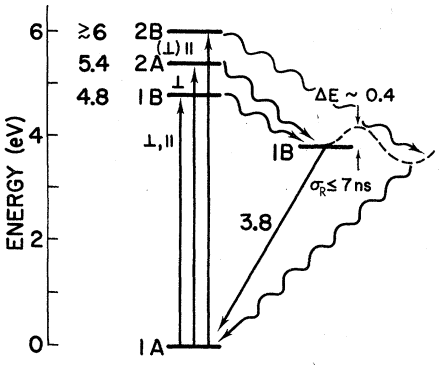

FIG. 7. Schematic representation of the F^+-center energy levels with polarization and peak energy values of the observed transitions. The 0.4-eV energy barrier to a nonradiative (or at least $h\nu \leq 1.5$ eV) decay channel obtains from the temperature dependence of the integrated emission intensity.

The 5.4-eV band induced by γ irradiation, however, was reported by Levy[6] to have a room-temperature FWHM of 1.25 eV, considerably broader than the particle-induced band with FWHM of 0.34 eV (Fig. 1 and Refs. 3 and 6). Furthermore, Levy observes that the intensity of this broad band begins to saturate near 3×10^4-R ^{128}Ta ($E_\gamma \sim 0.56$ MeV) exposure whereas the narrow band appears to grow with fusion dose[25] up to 1.4×10^{17} 14-MeV neutrons/cm^2 and with fission dose[6] up to a few times 10^{17} neutrons/cm^2, the highest doses reported for optical damage studies.

C. $1A \rightarrow 2B$ transition

In addition to the $1A \rightarrow 1B$ and $1A \rightarrow 2A$ transitions, the F^+ center in alumina is predicted to have a third transition from the $1A$ ground state to the $2B$ excited state.[7] From the theory the $1A \rightarrow 2B$ transition is expected to be relatively strongly polarized $\vec{E} \parallel \vec{c}$ as is shown in Table IV. The room-temperature absorption data in Fig. 1 does indeed show a shoulder at about 6.3 eV with this expected anisotropy. The excitation spectra for the 3.8-eV emission shown in Fig. 1, however, do not indicate a well-defined band at this energy. With the assumption that the $1A \rightarrow 2B$ transition has access to channels of nonradiative decay that are not available to the lower energy transitions, tentative assignment of the 6.3-eV shoulder to the $1A \rightarrow 2B$ transition of the F^+ center may be made. However, further work is required in order to substantiate this assignment.

D. Defect concentration

The volume concentration N of F^+ centers can be estimated using the calculated oscillator strengths and Smakula's equation,[26] $N_{F^+} f = 0.87 \times 10^{17}[n/(2+n^2)^2]\alpha H$, where n is the index of refraction at the absorption band peak, α is the maximum absorption coefficient, H is the band FWHM (in eV), and f the oscillator strength (see Sec. IV A). Calculating separately from Fig. 1 for the 4.8- and 5.4-eV bands for $\vec{E} \perp \vec{c}$ and the 4.8-eV band for $\vec{E} \parallel \vec{c}$ and averaging the three numbers, we obtain a value $N_{F^+} = 10.7 \times 10^{16}$ cm^{-3} for an incident flux of 3.9×10^{16} 14-MeV neutrons/cm^2.

An estimate for the F center concentration can also be obtained by assuming an oscillator strength for the F center that is twice[27] as large as the total oscillator strength to the $2p$ levels of the F^+ center; i.e., $f_F = 1.3$. Based on a comparison of the integrated intensities of the 4.8- and 6-eV absorption bands in Fig. 1(a) in conjunction with the calculated oscillator strengths for the $1A \rightarrow 1B$ and $1A \rightarrow 2B$ transitions listed in Table IV, ~90% of the prominent 6-eV band for $\vec{E} \perp \vec{c}$ may be taken as due to F centers; $N_F = 18.5 \times 10^{16}$ cm^{-3} is obtained for a flux of 3.9×10^{16} 14-MeV neutrons/cm^2. Total estimated errors are on the order of ±30%.

E. Emission-temperature dependence

The broad band that is observed for the 3.8-eV luminescence arises because the trapped electron interacts with a whole spectrum of normal modes of the defect lattice. The temperature dependence of the emission band FWHM, $H(T)$, is described by the expression[20]

$$H^2(T) = H^2(0)\coth(h\bar{\nu}/2kT) , \quad (1)$$

where $H(0)$ is the FWHM at low temperature, and $\bar{\nu}$ is a weighted average over the frequencies of all the defect-lattice modes that couple to the $1B$ electronic state. The dots in Fig. 8 show the tem-

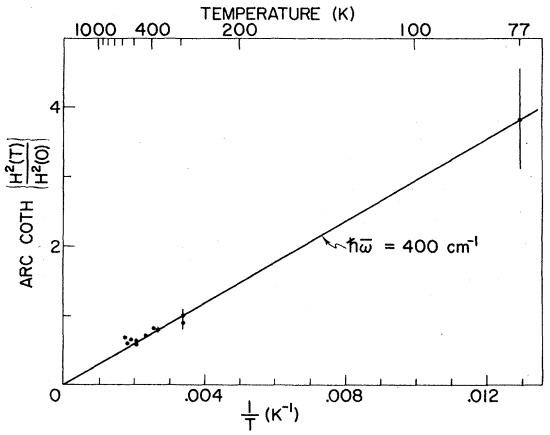

FIG. 8. Temperature dependence of the emission-band FWHM. The straight line represents Eq. (1) with $h\bar{\nu} = 400$ cm^{-1} and $H(0) = 0.343(5)$ eV.

perature dependence of the emission band FWHM. A good fit of Eq. (1) to the data is shown as the straight line in Fig. 8 and yields $h\bar{\nu} = 400 \pm 10$ cm^{-1} and $H(0) = 0.343(5)$ eV. This value for $h\bar{\nu}$ is not unreasonable since it lies close to bulk corundum acoustic modes reported at 378 and 432 cm^{-1}.[28] Moreover, frequencies determined in a similar manner for the F^+ centers in CaO and MgO also lie near high density-of-states points in the acoustic branch of the crystal phonon spectrum.[18,29-31]

The temperature dependence of the luminescence quantum efficiency for a simple system with only two decay channels, one radiative and the other nonradiative, from the relaxed excited state can be expressed as[20]

$$\eta(T) \propto [1 + \tau_R \nu_0 \exp(-\Delta E/kT)]^{-1} . \quad (2)$$

Here, τ_R is the radiative lifetime at low temperature, ΔE is the energy barrier to the nonradiative decay route, and ν_0 is a jump frequency. (The proportional sign is used because other nonradiative decay channels must be available before the system reaches the relaxed excited state since the low-temperature quantum efficiency is less than unity; see Sec. III B.) Because Eq. (2) is not very sensitive to $\tau_R \nu_0$, an estimate of this quantity is obtained first as $\tau_R \nu_0 \sim 4 \times 10^4$ from the calculated τ_R (see Sec. IV G), and taking $\nu_0 = \bar{\nu}$. Then, a good fit of Eq. (2) is obtained with $\Delta E = 0.4$ eV shown as the solid curve (a) in Fig. 3. This thermal barrier to a nonradiative channel out of the $1B$ state is depicted as the dashed curve in Fig. 7.

F. Huang-Rhys factor

The Huang-Rhys factor S, a parameter used to describe the strength of the linear electron-lattice interaction, is related to the second moment of the emission-band shape function by[32] $S = \langle E^2 \rangle / (h\bar{\nu})^2$. A value of $S = 11.2$ is obtained using the experimental second moment listed in Table IV (Appendix B) and the effective vibronic frequency determined in Sec. IV E. [It is noted that the assumption of a pure Gaussian band shape would lead to[18] $S = H^2(0)/(h\bar{\nu})^2 8 \ln 2 = 8.65$.] A relative estimate for the Huang-Rhys factor can be obtained on the basis of a semiclassical configuration coordinate diagram.[20] With the assumption of parabolic potential curves and equal ground- and excited-state effective vibronic frequencies, the low-temperature Stokes shift is given as $E_a - E_e = h\bar{\nu}(2S - 1)$; insertion of the experimental quanties yields $S = 10.8$, in excellent agreement with the value derived from the moments analysis.

The magnitude of the Huang-Rhys factor is related to the possibility of observing a zero-phonon line in absorption and emission. The ratio of integrated intensities of the zero-phonon line to the broad-band is expected[18] to be e^{-S}. Failure to observe a zero-phonon line near 4.3 eV in moderately high-resolution absorption ($\Delta\lambda \sim 0.05$ nm) and emission ($\Delta\lambda \sim 0.8$ nm) spectra taken near 10 K demonstrates that $S \geq 6.5$, in agreement with the above estimates. The Huang-Rhys factor for the F^+ center in Al_2O_3, therefore, lies intermediate between the strong coupling reported for MgO ($S \approx 35 \pm 5$) and the weak coupling reported for CaO ($S \sim 5$).[29-31]

G. Lifetime

The point-ion wave functions from Ref. 7 also provide an estimate for the lifetime of the $1B \rightarrow 1A$ emission of the F^+ center using the relationship[20]

$$\tau_R^{-1} = (2.68 \times 10^9) n E_e^3 (\mathcal{E}_{\text{eff}}/\mathcal{E}_0)^2 |\langle 1B|r|1A\rangle|^2 , \quad (3)$$

where n is the index of refraction at the emission band peak E_e. In Eq. (3), τ_R is in seconds while all other quantities are in Slater atomic units. With the choice[27] $\mathcal{E}_{\text{eff}}/\mathcal{E}_0 = 1$ and using unrelaxed wave functions[7] in the matrix element, the predicted lifetime is $\tau_R = 3.76$ nsec, consistent with the experimental observation of $\tau_R < 7$ nsec.

V. SUMMARY

Absorption and emission bands due to the F^+ center in fusion-neutron-irradiated sapphire have been identified. The absorption bands at 4.8 and 5.4 eV were assigned to the $1A \rightarrow 1B$ and $1A \rightarrow 2A$ transitions of the F^+ center, respectively, and the 3.8-eV luminescence band was assigned to the $1B \rightarrow 1A$ transition. A shoulder which appeared at ~6.3 eV for $\vec{E} \| \vec{c}$ was tentatively assigned to the $1A \rightarrow 2B$ transition; however, most of the prominent 6-eV absorption was assigned to the F center in agreement with the results of Lee and Crawford.[12]

The anisotropies of the F^+-center absorption bands have been measured at low temperature. In addition, a number of characteristics of the 3.8-eV emission were presented including quantum efficiency, lifetime, and temperature dependence. These optical properties of the F^+ center were found to be in good agreement with properties predicted from the point-ion wave functions of La, Bartram, and Cox.[7]

ACKNOWLEDGMENTS

The authors gratefully acknowledge Professor R. H. Bartram for stimulating and critical discussions. Additional discussions with Professor J. H. Crawford, Jr. are also acknowledged. J. M. Bunch and F. W. Clinard, Jr. are acknowledged

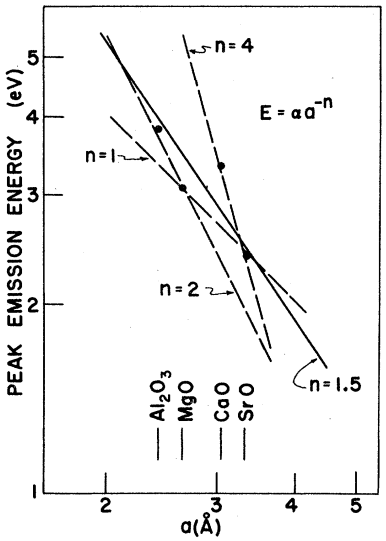

FIG. 9. Mollwo-Ivey plot for oxide F^+-center emission.

for the gracious loan of fusion-neutron-irradiated samples, and the Analytical Chemistry Group at Los Alamos Scientific Laboratory is acknowledged for impurity analysis of Czochralski sapphire. R. A. Van Konynenburg and other members of the Lawrence Livermore Laboratory are thanked for fusion neutron dosimetry. We thank H. Hendricks and other members of the NASA Langley Research Center for proton irradiations and D. W. Angel for preparations of sodium salicylate films. One of us (M. S.) received support as an NRC-NRL Resident Research Associate.

APPENDIX A: BULK-LATTICE EXPANSION CONTRIBUTION TO THE EMISSION-PEAK SHIFT

A contribution to the shift in the peak energy of emission with temperature can be considered to arise from thermal expansion of the lattice. In order to estimate this contribution consider $\partial E/\partial T = (\partial E/\partial a)(da/dT)$, where da/dT is the thermal expansion. In lieu of hydrostatic measurements, $\partial E/\partial a$ will be estimated from a Mollwo-Ivey relation.[20]

The Mollwo-Ivey relation is derived from a particle-in-a-box model for the electron(s) trapped at an anion vacancy where it is assumed that the ground to first-excited-state transition scales with the lattice parameter a, as $E = \alpha a^{-n}$. An infinite-square-well potential gives $n = 2$ while a finite potential well and the inclusion of polarization effects places n in the range $1 \leq n \leq 2$.[33] This simple model works "well" for F-center absorption bands in alkali halides for which a value of $n = 1.84$ has been reported.[20] However, results for F-center emission bands yield a less satisfactory value[20] of $n \sim 2.5$; the applicability of the Mollwo-Ivey relation is doubtful for $n > 2$.[34] Initial and provocative results have also been reported for defect center absorption bands in oxides.[35,36]

Figure 9 is a plot of the F^+-center emission peak versus (oxygen density)$^{-1/3}$ for oxide crystals where the F^+-center emission has been well established.[18,29,37,38] [The near-neighbor distance is taken to be (oxygen density)$^{-1/3}$ because materials with different crystal structures are compared.[36]] The dashed lines show that selected data points can be fit with values of n ranging from 1 to 4. The large deviations from a straight line shown in Fig. 9 indicate that details of the local potential cannot be ignored in any realistic prediction of the emission-band peak position.[33,34]

The solid line in Fig. 9 with $n = 1.5$ and $\alpha = 14.9$ is adequate for our purposes, however, and provides a reasonable estimate for $\partial E/\partial a$. An isotropic average of $da(T)/dT$ over the range $0 \leq T \leq 600$ K was obtained from the experimental work of Kirby.[39] The estimated net lattice effect on the emission-band peak position is indicated by the dashed curve in Fig. 4.

TABLE V. Emission-band moments at 77 K.

Moment		Value
Zeroth:	$\int g(E)\,dE$	1 [a]
First:	$\bar{E} = \int Eg(E)\,dE$	3.82(7) eV
First about $\bar{E}$:	$\langle E \rangle = \int (E-\bar{E})g(E)\,dE$	−0.0409 eV [b]
Second about $\bar{E}$:	$\langle E^2 \rangle = \int (E-\bar{E})^2 g(E)\,dE$	0.0275 eV^2

[a] For normalized line-shape function.
[b] Equals zero for a Gaussian $g(E)$.

APPENDIX B: EMISSION-BAND MOMENTS ANALYSIS

Einstein's coefficient for spontaneous emission at energy E_e can be expressed as[20]

$$A = \left[\left(\frac{\mathcal{E}_{\text{eff}}}{\mathcal{E}_0}\right)^2 n\right] \frac{4e^2}{3\hbar^4 c^3} E_e^3 g(E)\ , \tag{4}$$

where

$$g(E) = a v_b \sum_a |\langle a|r|b\rangle|^2 \delta(E_b - E_a - E)\ . \tag{5}$$

That is, $g(E)$ is a thermal average over the initial

(excited) vibronic states and a sum over the final (ground) vibronic states. However, the quantity that is observed experimentally is the luminescence intensity $I(E) = NE_e A$. All moments listed in Table V are computed for the band-shape function $g(E)$; however, for narrow bands the normalized moments of $I(E)$ are the same within experimental uncertainty.

[1]D. G. Martin, J. Phys. Chem. Solids 10, 64 (1958).
[2]J. J. Antal and A. N. Goland, Phys. Rev. 112, 103 (1958). (1958).
[3]E. W. J. Mitchell, J. D. Rigden, and P. W. Townsend, Philos. Mag. 5, 1013 (1960).
[4]F. T. Gamble, R. H. Bartram, C. G. Young, and O. R. Gilliam, Phys. Rev. 138, A577 (1965).
[5]G. W. Arnold and W. D. Compton, Phys. Rev. Lett. 4, 66 (1960).
[6]P. Levy, Phys. Rev. 123, 1226 (1961).
[7]S. Y. La, R. H. Bartram, and R. T. Cox, J. Phys. Chem. Solids 34, 1070 (1973).
[8]J. M. Bunch and F. W. Clinard, Jr., J. Am. Ceram. Soc. 57, 279 (1974).
[9]G. W. Arnold, G. B. Krefft, and C. B. Norris, Appl. Phys. Lett. 25, 540 (1974).
[10]B. D. Evans, H. D. Hendricks, F. D. Bassarre, and J. M. Bunch, in *Ion Implantation in Semiconductors, 1976,* edited by F. Chernow, J. A. Borders, and D. K. Brice (Plenum, New York, 1977), p. 265.
[11]T. J. Turner and J. H. Crawford, Jr., Solid State Commun. 17, 167 (1975).
[12]K. H. Lee and J. H. Crawford, Jr., Phys. Rev. B 15, 4065 (1977).
[13]Y. Chen, J. L. Kolpus, and W. A. Sibley, Phys. Rev. 186, 865 (1969).
[14]L. A. Kappers, R. L. Kroes, and E. B. Hensley, Phys. Rev. B 1, 4151 (1970).
[15]R. A. Van Konynenburg, Lawrence Livermore Laboratory Report No. UCRL-51393 Rev. 1, May 24, 1974 (National Technical Information Service, Springfield, Va. 22151).
[16]H. H. Tippins, Phys. Rev. B 1, 126 (1970).
[17]R. Allison, J. Burns, and A. J. Tuzzolino, J. Opt. Soc. Am. 54, 747 (1964).
[18]A. E. Hughes and B. Henderson, in *Point Defects in Solids*, Vol. 1, edited by J. H. Crawford, Jr. and L. M. Slifkin (Plenum, New York, 1972), p. 381.
[19]D. W. Muir and J. M. Bunch, Proceedings of the International Conference on Radiation Effects and Tritium Technology for Fusion Reactors, Gatlinburg, Tenn., 1–3 Oct. 1975 (USERDA CONF 750989, National Technical Information Service, Springfield, Va. 22151), Vol. II, p. 517.
[20]*Physics of Color Centers*, edited by W. B. Fowler (Academic, New York, 1968), Chaps. 2 and 6.
[21]K. H. Lee and J. H. Crawford, Jr., Appl. Phys. Lett. 33, 273 (1978).
[22]W. C. Ward and E. B. Hensley, Phys. Rev. 175, 1230 (1968).
[23]B. P. Johnson and E. B. Hensley, Phys. Rev. 180, 931 (1969).
[24]Y. Chen, R. T. Williams, and W. A. Sibley, Phys. Rev. 182, 960 (1969).
[25]J. M. Bunch (private communication).
[26]D. L. Dexter, Solid State Phys. 6, 353 (1958).
[27]D. Y. Smith and D. L. Dexter, Prog. Optics X, 165 (1972).
[28]W. Kappus, Phys. B 21, 325 (1975).
[29]B. D. Evans and J. C. Kemp, Phys. Rev. B 2, 4179 (1970).
[30]A. E. Hughes, J. Phys. C 3, 627 (1970).
[31]Y. Merle d'Aubigné and A. Roussel, Phys. Rev. B 3, 1421 (1971).
[32]M. Lax, J. Chem. Phys. 20, 1752 (1952).
[33]R. F. Wood, J. Phys. Chem. Solids 26, 615 (1965).
[34]W. Hayes and A. M. Stoneham, Phys. Lett. A 29, 519 (1969).
[35]T. J. Turner, Solid State Commun. 7, 635 (1969).
[36]J. M. Bunch, Phys. Rev. B 16, 724 (1977).
[37]T. M. Wilson and R. F. Wood, J. Phys. (Paris) 37, C7–190 (1976).
[38]J. Feldott, G. P. Summers, T. M. Wilson, H. T. Tohver, M. M. Abraham, Y. Chen, and R. F. Wood, Solid State Commun. 25, 839 (1978).
[39]R. K. Kirby, in Proceedings of the Symposium on the Mechanical and Thermal Properties of Ceramics, Gaithersburg, Md., 1-2 April 1968, edited by J. B. Wachtman, Jr. (NBS Special Pub. 303), p. 41.